

Wettability-dependent Wave Velocities and Attenuation in Granular Porous Media

Jimmy Xuekai Li¹, Reza Rezaee², Tobias M. Müller³, Mahyar Madadi⁴, Rupeng Ma⁵, and Mohammad Sarmadivaleh¹

¹Curtin University

²Curtin University

³Department of Seismology

⁴The University of Melbourne

⁵Hohai University

November 26, 2022

Abstract

Understanding wave propagation in granular sediments is important for subsurface characterization. The presence of fluid and wettability condition result in additional complexities. While it is known that wave propagation in dry granular porous media is dominated by the presence of force chains, their influence in (partially) saturated granular porous media with different wettability conditions remains largely unexplored. To make progress in this direction, we design laboratory experiments by combining core flooding and ultrasonic measurement in glassbead packings that are chemically treated to alternate the wettability. The P- and S-wave velocity-saturation relation and attenuation-saturation relation are obtained from the waveforms for both water- and gas-wetting samples. The results show that there is a transition from an attenuating but stable P-wave pulse at low and moderate saturation to a set of incoherently scattered waves at high saturation. The incoherent scattering in the gas-wetting case is negligibly small, whereas it is more pronounced in the water-wetting case. We conclude that only if water wets the grains, can the liquid enter the grain contacts. These liquid bridges are thought to locally reinforce the force chains and to increase their characteristic length scale. This leads to an increase in P-wave velocity and promotes incoherent scattering since the ratio of dominant wavelength to characteristic length scale decreases. In the gas wetting case, however, the presence of gas prevents the water from direct contact with the glass beads and therefore stops the formation and growth of the liquid bridges within the force chain network.

Wettability-dependent Wave Velocities and Attenuation in Granular Porous Media

Jimmy X. Li¹, Reza Rezaee¹, Tobias M. Müller^{2,3}, Mahyar Madadi⁴, Rupeng
Ma³ and Mohammad Sarmadivaleh¹

¹Western Australian School of Mines, Curtin University, Kensington, WA 6151, Australia.

²Department of Seismology, Centro de Investigacion Cientifica y de Educacion Superior de Ensenada,
22860 Ensenada, BC, Mexico.

³School of Earth Sciences and Engineering, Hohai University, Nanjing 211100, China.

⁴School of Mathematics and Statistics, The University of Melbourne, Parkville, VIC 3010, Australia.

Key Points:

- The first experimental investigation of wettability effect on the wave phenomena in granular porous media with variable water saturation.
- The wettability affects the wave velocity and attenuation by controlling the spatial distribution of fluids.
- The wave scatterings in granular porous media are linked to wettability and saturation.

Corresponding author: Jimmy X. Li, Jimmy.Li@postgrad.curtin.edu.au, 26 Dick Perry Avenue, Kensington, WA 6151, Australia.

Abstract

Understanding wave propagation in granular sediments is important for subsurface characterization. The presence of fluid and wettability condition result in additional complexities. While it is known that wave propagation in dry granular porous media is dominated by the presence of force chains, their influence in (partially) saturated granular porous media with different wettability conditions remains largely unexplored. To make progress in this direction, we design laboratory experiments by combining core flooding and ultrasonic measurement in glassbead packings that are chemically treated to alternate the wettability. The P - and S -wave velocity-saturation relation and attenuation-saturation relation are obtained from the waveforms for both water- and gas-wetting samples. The results show that there is a transition from an attenuating but stable P -wave pulse at low and moderate saturation to a set of incoherently scattered waves at high saturation. The incoherent scattering in the gas-wetting case is negligibly small, whereas it is more pronounced in the water-wetting case. We conclude that only if water wets the grains, can the liquid enter the grain contacts. These liquid bridges are thought to locally reinforce the force chains and to increase their characteristic length scale. This leads to an increase in P -wave velocity and promotes incoherent scattering since the ratio of dominant wavelength to characteristic length scale decreases. In the gas wetting case, however, the presence of gas prevents the water from direct contact with the glass beads and therefore stops the formation and growth of the liquid bridges within the force chain network.

Plain Language Summary

The distinction of waveforms from the acoustic measurement of granular porous media with different wettability demonstrates that wettability has a significant influence on wave propagation. This is because the spatial distribution of the fluids is controlled by wettability. Only if the sample is water wetting, the liquid can occupy grain contacts. These liquid-reinforced grain contacts result in higher velocities, less attenuation. In addition, the spatial arrangement of the liquid-reinforced grain contacts is thought to change the characteristic length scale of the force chains. This can lead to the scattering of wave pulses when their dominant wavelengths are comparable to the characteristic length scale.

1 Introduction

Since granular porous media define zones with high porosity and permeability they are important for freshwater aquifer characterization, oil and gas production, and CO_2 geo-sequestration. Hence, there is a wide genre of scientific interests in the properties of granular porous media, including their acoustic properties (C.-h. Liu & Nagel, 1992; Melosh, 1996; Scott, 1996; P. A. Johnson & Jia, 2005; Parra et al., 2006; Moebius et al., 2012; Lo & Sposito, 2013; Güven et al., 2018). In the context of groundwater exploitation and exploration geophysics, soft and unconsolidated sediments (e.g. soil and sand packings) in the subsurface are often conceptualized as fluid-saturated granular porous media. In particular, for the interpretation of sonic and seismic data it is important to understand their overall elastic properties, velocity dispersion, and attenuation mechanisms (Anthony & Marone, 2005; Daniels & Hayman, 2008; T. Dutta et al., 2010).

It is known that for porous media saturated with more than one fluid the wave velocity is not only dependent on the saturation, i.e., the volumetric proportion, but also dependent on the fluid distribution, i.e., the geometrical arrangement and length scales of fluid pockets. In this regard, there have been several experiments to study the velocity-saturation-relation (VSR) in various lithologic rocks with mixed liquid-gas saturation (Murphy III, 1984; Cadoret et al., 1995; Lebedev et al., 2009; Alemu et al., 2013; Lopes et al., 2014). These VSR can be often constrained by the two end-member models of patchy and uniform saturation. They correspond to the upper bound and lower bound velocities de-

67 scribed by the Gassmann-Hill (GH) and Gassmann-Wood (GW) equations, respectively (Toms
68 et al., 2006). Similar experiments for granular porous media are not known. Even the
69 applicability of the GW and GH bounds in partially saturated granular porous media
70 remains unclear. Nonetheless, it is known that wave velocities are strongly different in
71 dry and saturated granular porous media (Job et al., 2008; Brunet et al., 2008; Griffiths
72 et al., 2010). Therefore, one can expect a pronounced signature of partial saturation to
73 be present in granular porous media as well.

74 As far as velocity dispersion and attenuation in partially saturated rocks are con-
75 cerned, there are multiple models to account for wave-induced-fluid-flow (WIFF), which
76 is thought to be a relevant dissipation mechanism caused by the relative motion of solid
77 and fluid (White, 1975; N. Dutta & Odé, 1979; Santos et al., 1990; Mavko & Mukerji,
78 1998; D. L. Johnson, 2001; Müller & Gurevich, 2004; Lo et al., 2005; Ba et al., 2011; Sun
79 et al., 2018). These models are used to interpret observed VSRs that do not follow ei-
80 ther the GH or GW bounds, but show trends in between these bounds. These WIFF mod-
81 els also allow us to interpret the attenuation-saturation relation (ASR) (Qi et al., 2014;
82 J. Liu et al., 2016). While it is known that waves in granular porous media become at-
83 tenuated, one may expect additional attenuation in partially saturated granular porous
84 media (Brunet et al., 2008). However, the precise nature of WIFF in granular porous
85 media is unknown, and therefore the applicability of one of the above-mentioned mod-
86 els remains questionable.

87 The presence of two fluids inevitably implies that two-phase flow concepts such as
88 capillarity and wettability become relevant. For example, Qi et al. (2014) find that cap-
89 illarity stiffening may result into higher wave velocities and accordingly modify the GW
90 bound based on ideas earlier suggested by Nagy and Blaho (1994) and Tserkovnyak and
91 Johnson (2003). Lo et al. (2017) discover the dynamic response of the water retention
92 curve (relationship of capillary pressure and water saturation) during water drainage in
93 unsaturated porous media under acoustic excitation. The wettability as an interfacial
94 phenomenon is thought to be a key factor controlling the spatial distribution of fluids.
95 Their location and displacement will have significant influence on the capillary pressure,
96 relative permeability, and water-flooding performance (Anderson, 1987; Anderson et al.,
97 1987a, 1987b; Bultreys et al., 2016; Khishvand et al., 2017; Hu et al., 2017).

98 However, in none of the above-mentioned studies, the wettability of the porous me-
99 dia has been considered. Ignoring the wettability impact on wave propagation may lead
100 to errors and misinterpretation of experimental and field test results. Therefore, in an
101 attempt to understand the effect of wettability on waves velocities, we aim at experiments
102 in an idealized porous medium, in which we can have full control of the wettability. For
103 this purpose, we choose glass bead packings as a particular simple representation of a
104 granular porous medium.

105 Although there are a lot of similarities between granular porous medium and rigid
106 porous medium and some poroelastic theories may be applicable to the granular porous
107 medium, the grains in granular porous medium have additional degree of freedom com-
108 pared to the solid frame of consolidated rigid porous media. In non-cohesive granular
109 porous media under external stress, some grains are load-bearing, others not. This re-
110 sults in an inhomogeneous pattern of load-bearing grains, the so-called force chain net-
111 works. Force chain networks can be directly observed by photo-elastic visualization ex-
112 periments (Howell et al., 1999; Owens & Daniels, 2011; Ladd & Reber, 2020).

113 Since the contact force chain network bears the strongest stress on the direction
114 of the compression, it dominates the mechanical properties of granular porous media,
115 including the elastic response to the external disturbance such as acoustical perturba-
116 tion (C. M. Sayers, 2021). When the granular porous medium is saturated by two im-
117 miscible fluids, the grain contacts are always occupied by the wetting fluid because of
118 the capillary action, while the non-wetting fluid is forced into the relatively larger pores (Anderson

119 et al., 1986). Such a wettability-dependent spatial distribution of fluids is most likely to
 120 affect the structure of the force chain network. Different from the dry Hertzian contacts,
 121 the presence of the liquid bridges in the grain contacts (i.e. the water bridges in the water-
 122 wetting sample) induce the elasto-hydrodynamic collision of grains under ultrasonic fre-
 123 quency, which consequently increase the stiffness of the contact, enlarge the force chain
 124 network and therefore increase the characteristic length of the force chains (Davis et al.,
 125 1986; Job et al., 2008).

126 In this paper, we explore the wettability effect on the wave propagation in the (par-
 127 tial) saturated granular porous media by the experiments combining acoustic measure-
 128 ment and core flooding. We first present the experiment setup and results. The wave-
 129 form of the P - and S -wave on each step of incremental water injection (increase of wa-
 130 ter saturation) are recorded for both water-wetting and gas-wetting glass bead packings.
 131 The velocity-saturation-relation (VSR) and attenuation-saturation-relation (ASR) are
 132 extracted from the waveforms. Then, the wettability dependent scattering patterns are
 133 identified for two samples with different wettability. A wettability-dependent character-
 134 istic length of the force chains is used to interpret the wave scattering observations and
 135 the piece-wise function of effective bulk and shear moduli are proposed to simulate the
 136 transition from coherent wave in dry or low saturation to incoherent wave in high and
 137 full saturation.

138 2 Experimental Setup

139 The experimental setup consists of a poly-carbonate cylinder (15.5 mm inner di-
 140 ameter and 48–52 mm length) packed with spherical glass beads with a quasi-identical
 141 diameter of $200 \pm 50 \mu\text{m}$ and two piston piezoelectric acoustic transducers mounted on
 142 the two ends. This is the typical configuration to carry out acoustic measurements in
 143 granular materials (P. A. Johnson & Jia, 2005). The fluid can be injected through the
 144 inlet line and the displaced fluid exits through the outlet line (Figure 1). Olympus V103
 145 and V153 piezoelectric transducers with broadband frequency range 0.2–2 MHz and
 146 1 MHz nominal (center) frequency are used to generate and receive P - and S -wave pulses,
 147 respectively. A uniaxial pressure of about 150 kPa is applied on the outside faces of the
 148 transducers to guarantee dense packing.

149 To indicate the wettability the contact angle is measured. The water droplets are
 150 applied on the original glass surface and the Quilon-C treated surface, respectively, in
 151 the air environment. The measured contact angle is on a water-air-glass interface is 7.64° ,
 152 which is far less than 90° indicating that the pure, untreated glass beads are strongly
 153 water-wetting (Figure 2). The water is incrementally injected into the packing through
 154 the inlet line with an approximate flow rate of 0.7 ml/s . The acoustic measurement is
 155 conducted after each incremental injection. The change of water saturation is precisely
 156 captured by measuring the weight of the sample.

157 The same injection-measurement procedure is performed on the glass bead pack-
 158 ing when the wettability is altered in order to have gas wetting glass beads. Quilon-C
 159 in isopropyl alcohol solution is used to alter the wettability of the original water-wetting
 160 glass beads to be gas-wetting by following the same procedures outlined in the litera-
 161 ture (Garrouh & Sharma, 1995). The chemical contains C-14-C-18 fatty acids with chromium,
 162 which bonds the negatively charged glass bead surface rendering a gas-wetting (hydropho-
 163 bic) thin coating on the spheres. An advantage of such treatment is that there is little
 164 impact on the porosity of the fully saturated porous medium (Garrouh & Alikhan, 1997).
 165 We find that the porosity of glassbead packing changes from 38.5% as original hydrophilic
 166 condition to 37.5% as processed hydrophobic condition. The hydrophobicity or gas-wetting
 167 condition is confirmed by a 105.5° measured contact angle on the water-air-glass inter-
 168 face after the Quilon-C chemical treatment (Figure 2).

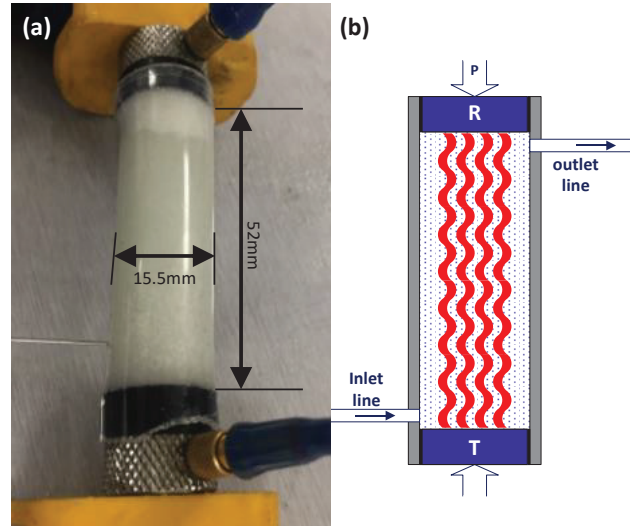


Figure 1. (a) Real and (b) schematic experimental set-up for conducting acoustic measurement during the water-air core flooding in the glass bead pack under axial pressure P . T and R denote the piezoelectric transmitter and receiver, respectively.

169 While the porosity and permeability are not significantly changed due to the chem-
 170 ical treatment, the mechanical properties are expected to change. In the case of water-
 171 wetting glass bead packing, the sample can be thought as uncoated, only held together
 172 by the enclosure of sleeve and the uniaxial compression applied. However, in the gas-wetting
 173 glass bead packing, the water-repellent coating and the possible residual chemical de-
 174 position on the glass beads as demonstrated in Figure (2b) act as coating layers. They
 175 strengthen the entire stiffness of the gas-wetting glass bead packing (Dvorkin et al., 1991,
 176 1994). This is confirmed by the observation that the P -wave velocity of dry gas-wetting
 177 glass bead packing is higher than the value of dry water-wetting sample (Figure 5 and
 178 6).

179 3 Experimental Results

180 3.1 Water-wetting Case

181 Seismograms of P - and S -waves are recorded separately for the water-wetting sam-
 182 ple for each saturation step (Figure 3). We observe that in the P -wave transmission ex-
 183 periment (Figure 3a) there is a clear transition from a stable coherent wave pulse towards
 184 a set of incoherent scattering waves with shorter wavelengths for increasing water sat-
 185 uration. With incremental water injection, initially the traveltime of the first arrival slightly
 186 increases and the amplitude decreases slowly until a critical water saturation $S_c \approx 89\%$
 187 is reached. Beyond this critical saturation the traveltime becomes very short and the am-
 188 plitude increases sharply. For the S -wave transmission experiment, there is only one co-
 189 herent pulse recognizable whose traveltime increases slightly with the increase of water
 190 saturation. Nevertheless, the P -wave arrival is visible on the S -wave measurement at low
 191 and intermediate water saturation (Figure 3b).

192 3.2 Gas-wetting Case

193 The gas-wetting glass beads are obtained from the original water-wetting beads treated
 194 by the wettability alteration agent Quilon-C. Better contact between glass beads is ex-

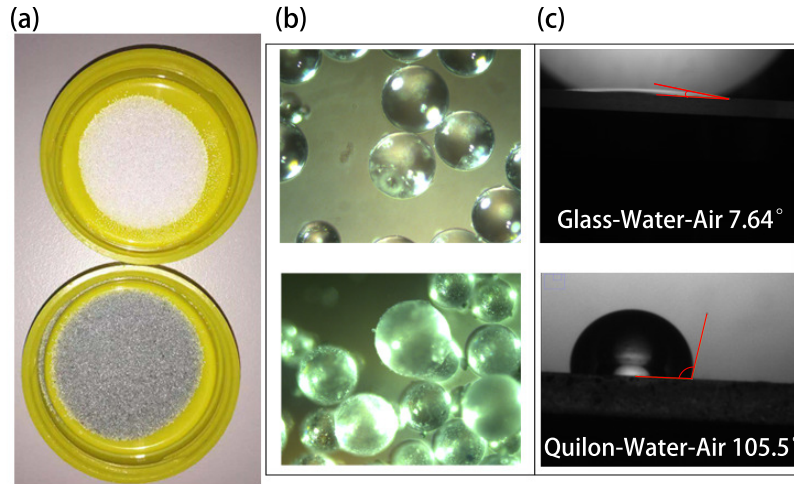


Figure 2. (a) Original glass bead sample (top) appearing in shiny white color and the Quilon-C treated glass bead sample (bottom) in dark green color; (b) microscopy images of the original glass beads and treated beads; (c) the corresponding contact angle of water droplet on original glass surface (top) is 7.64° and on the processed glass surface after Quilon-C chemical treatment (bottom) is 105.5° .

195 expected after the treatment. This is indeed corroborated since we observe higher ampli-
 196 tude and higher velocity for dry gas-wetting glass bead packing compared to the origi-
 197 nal water-wetting one. However, with the increase of water saturation, the gas wetting
 198 packing exhibits a strong damping effect and the waveforms of both P - and S -wave be-
 199 come attenuated drastically (Figure 4). The increase of water saturation stops around
 200 93%-94% in the standard water flooding procedure with about 6% residual gas satura-
 201 tion. After a three-fold increase of the injection pressure, we spot some of the suspected
 202 scattered P -waves after the critical water saturation $S_c \approx 98\%$, though the amplitude
 203 is very small (Figure 4a). The gas as wetting fluid phase is trapped inside the grain con-
 204 tact and is hardly displaced by the water in the standard water injection process. How-
 205 ever, the increased injection pressure may overcome the capillary pressure and thereby
 206 push the non-wetting water into some of the grain contacts.

207 4 Wettability Impact on the Velocity and Attenuation

208 The inferred velocity-saturation relation (VSR) of both P - and S -wave transmis-
 209 sion experiments are plotted in Figure 5 and 6 for the water-wetting and gas-wetting sam-
 210 ples, respectively. The results are compared with the Gassmann-Wood limit (lower bound
 211 for uniform saturation) and Gassmann-Hill limit (upper bound for patchy saturation),
 212 where the detailed formulas are given in Appendix A. The predictions of the Biot the-
 213 ory, i.e., for a fully saturated porous medium are also provided for reference. The pa-
 214 rameters of the samples are listed in Table 1. In addition, we calculate the attenua-
 215 tion-saturation relation for both transmission experiments. The attenuation is obtained via
 216 the spectral-ratio method with key formulas in Appendix B. The results are plotted in
 217 Figure 7.

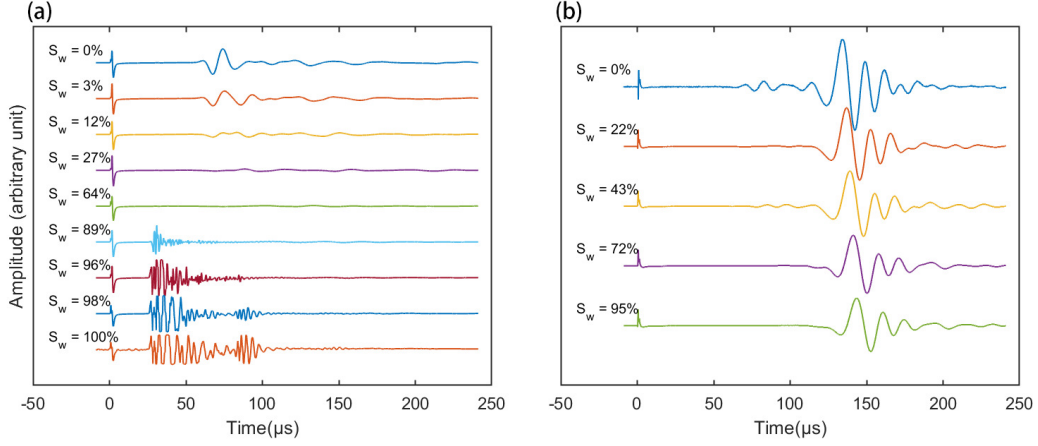


Figure 3. Recorded waveforms of (a) *P*-wave and (b) *S*-wave after incremental injection for water-wetting glass bead packing. The small peak at the $t=0$ is the cross-talk signal during the pulse generation.

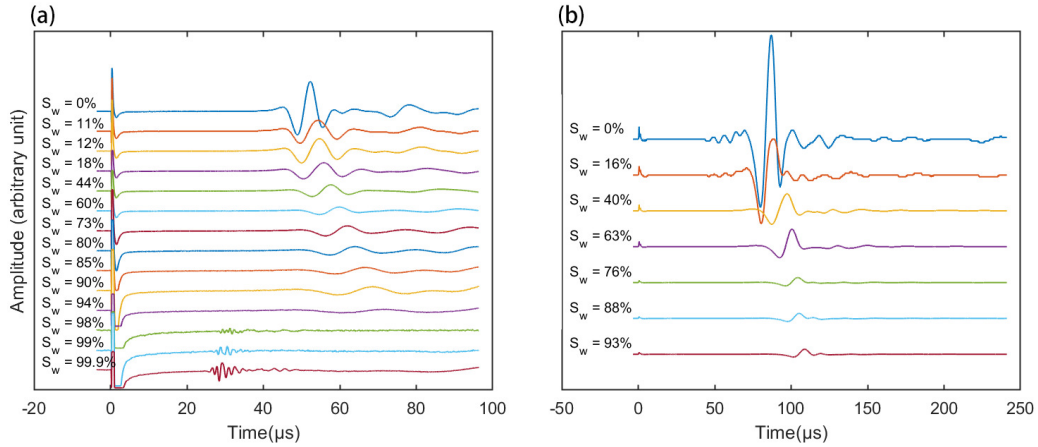


Figure 4. Recorded waveforms with incremental water injection for gas-wetting glass bead packing: (a) *P*-wave; (b) *S*-wave transmission experiments.

218

4.1 Water-wetting Case

219

220

221

222

223

224

225

226

227

228

229

230

231

232

For the water-wetting sample, water tends to occupy the glass bead surface and the grain contacts as soon as the fluid is fingering through the inter-granular voids. This favors the generation of capillary bridges (pendulum rings made of water). Initially, such capillary bridges may only appear in the finest and smallest pores. The water then quickly occupies the relatively large pores. At low- to intermediate water saturation, the capillary bridges are not fully established in all grain contacts. Therefore, the force chains are thought to form a discontinuous pattern like schematically indicated in inset of Figure 5. Then the *P*-wave VSR is closer to the prediction of Gassmann-Wood bound. At the same time, the attenuation of the *P*-wave (Figure 7a) becomes higher with increasing water saturation but the attenuation of the *S*-wave (Figure 7b) is less affected by the change of water saturation. Once the water saturation reaches a critical saturation (i.e., $S_c \approx 89\%$) and beyond, the force chains under ultrasonic frequency become reinforced and the grain contacts saturated by water form in a continuous percolating pattern (inset of Figure 5).

Table 1. Parameters of Glassbead Packing and the Injected Water

Water	
Density, ρ_w	997 kg/m^3
Bulk Modulus, K_w	2.25 GPa
Viscosity, μ_w	1 cP
Gas (air, 25 °C)	
Density, ρ_g	1.18 kg/m^3
Bulk Modulus, K_g	0.142 MPa
Solid	
Density, ρ_s	2455 kg/m^3
Bulk Modulus, K_s	37 GPa
Grain Diameter, d	200 μm
Water-wetting Matrix	
P - Wave Velocity, V_p	963.504 m/s
S - Wave Velocity, V_s	466.36 m/s
Porosity, ϕ	0.385
Tortuosity \dagger , T	1.8
Permeability \ddagger , κ	$3.37 \times 10^{-11} m^2$
gas-wetting Matrix	
P - Wave Velocity, V_p	1295.24 m/s
S - Wave Velocity, V_s	782 m/s
Porosity, ϕ	0.375
Tortuosity \dagger , T	1.83
Permeability \ddagger , κ	$3 \times 10^{-11} m^2$

\dagger Estimated by $T = \frac{1}{2}(1 + 1/\phi)$ (Berryman & Thigpen, 1985).

\ddagger Kozeny-Carman Permeability $\kappa = \frac{\phi^3}{180(1-\phi)^2}d^2$ (Xu & Yu, 2008).

233 This interstitial liquid-induced structural change of the force chains has paramount
234 impact on the velocity and the attenuation. On the one hand, it leads to higher effec-
235 tive elastic moduli (both bulk modulus and shear modulus) of matrix frame. Since the
236 composite density does not change appreciably, the corresponding P - and S -wave veloc-
237 ities at higher saturation are larger compared to the Gassmann theory predictions (Fig-
238 ure 5). On the other hand, the overall growth of the force chain network is accompanied
239 with a local clustering of grains connected via capillary bridges. These clusters, in turn,
240 can be characterized by a characteristic length which exceeds the individual grain size.
241 Once the characteristic length becomes comparable to the P -wavelength, the notion of
242 an effective medium is no longer valid. Instead, one expects that the P -wave are elas-
243 tically scattered at the clusters. This could explain the emergence of the incoherent wave
244 pulses seen in Figure 3. Given that the frequency range of the piezoelectric transducer
245 is 0.2 – 2 MHz , the P -wavelength ranges from 1 – 10 mm for either water-wetting or
246 gas-wetting samples in (near) full water saturation condition. However, the diameters
247 of the glass beads are much smaller, $d = 0.2 \pm 0.05 mm$. If the characteristic length of
248 the force chains is short-ranged ($\xi \sim d$) due to the gas filled grain contacts, there should

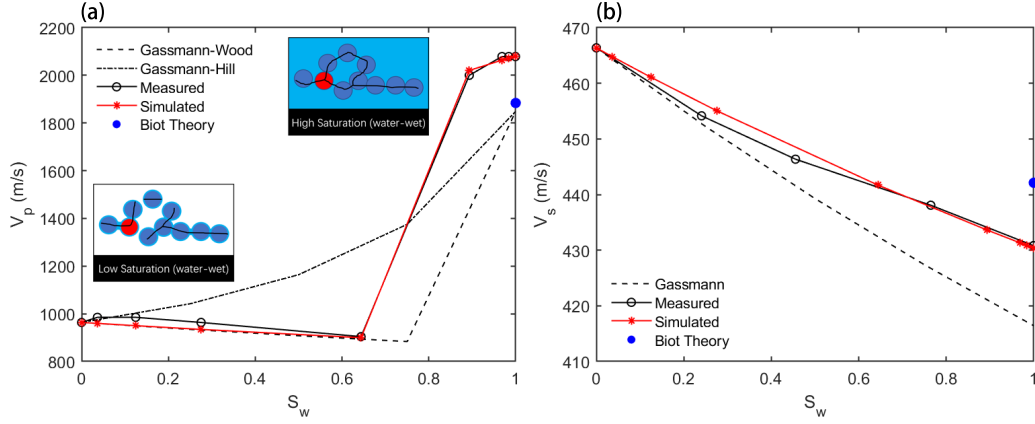


Figure 5. The measured velocity-saturation relation in water-wetting glass bead packing is compared with Gassmann-Wood and Gassmann-Hill theoretical predictions for (a) P -Wave and (b) S -Wave. As reference, Biot theory is used for calculation of the velocities of sample under full water saturation. The inset cartoons illustrate the network of force chain (black solid line) in low and fully saturated samples.

249 be little incoherent signals and a stable P -wave pulse is propagating. However, the ob-
 250 servation of the incoherently scattered waves in the water-wetting sample is suggestive
 251 for the existence of long-range characteristic length ($\xi \sim 5 - 10d$).

252 The appearance of these incoherently scattered waves is also clearly marked as a
 253 negative $1/Q_p$ in the P -wave attenuation-saturation relation (Figure 7a). The negative
 254 value is a consequence of using the spectral ratio method to determine Q . It essentially
 255 consists in dividing the amplitude spectrum of a waveform by a reference amplitude spec-
 256 trum (i.e., the signal in an aluminum core with the same length as the sample). This ref-
 257 erence amplitude spectrum is shown in Figure 8b (black line). The amplitude spectrum
 258 corresponding to the first period of a scattered wave in the water-wetting sample has two
 259 peaks (Figure 8b, red line). The center frequency that corresponds to the first peak (#1
 260 in Figure 8b) is lower than the center frequency of the reference amplitude spectrum.
 261 Computing the spectral ratio at this center frequency yields to a positive Q value. Con-
 262 versely, computing the spectral ratio at the center frequency of the second peak (#2 in
 263 Figure 8b) yields to a negative Q value. The changes in the force chain network due to
 264 the injection of the liquid bring the amplitude spectrum a bi-modal pattern, which con-
 265 tains not only low-frequency coherent waves but also high-frequency incoherent scatter-
 266 ing components (Figure 9a). These scattered waves are associated with a negative $1/Q$.
 267 In this sense, the Q factor does not quantify the amplification of a pulse but is an in-
 268 dication of the change of signal character.

269 The Gassmann-Wood predictions match the measured P -wave velocity reasonably
 270 well at low- to intermediate water saturation as long as the saturation is below the crit-
 271 ical water saturation S_c . At a water saturation beyond S_c , the force chain network is en-
 272 riched with unrelaxed grain contacts, where local pressure gradients induced by the wave
 273 are not equilibrated. Such a scenario resembles the high-frequency unrelaxed frame con-
 274 cept developed by Mavko and Jizba (1991) and described by the Mavko-Jizba relation.
 275 The basic idea is that the non-equilibrated wave-induced pressure perturbation at grain
 276 contact is incorporated in form of high-frequency unrelaxed "wet-frame" moduli K_{uf} and
 277 μ_{uf} . These moduli are higher compared to the moduli at low frequencies when the pres-
 278 sure gradients are equilibrated. We find that the Mavko-Jizba relations work well to pre-
 279 dict the P - and S -wave velocities of the fully saturated water-wetting sample as the wa-

280 ter occupies the grain contacts to form a "wet-frame". By taking advantage of the two
 281 end velocities (dry and full saturation), we are able to simulate the P -wave velocities at
 282 high saturation ($S_w \geq S_c$) and S -wave velocities by the Voigt averaged elastic mod-
 283 uli:

$$284 \quad K = \begin{cases} K_{GW}; & \text{if } S_w < S_c \\ K_d(1 - S_w) + K_{MJ}S_w & \text{if } S_w \geq S_c \end{cases} \quad (1)$$

$$285 \quad \mu = \mu_d(1 - S_w) + \mu_{MJ}S_w \quad (2)$$

287 where the K_{GW} are Gassmann-Wood limit of the bulk modulus of the partially saturated
 288 sample, K_{MJ} and μ_{MJ} are the bulk and shear moduli of the fully saturated sample by
 289 Mavko-Jizba relations, K_d and μ_d are the bulk and shear moduli of the drained (dry)
 290 sample. The simulated velocities match the measured velocities very well as demon-
 291 strated in Figure 5. We list the relevant formulas in Appendix A.

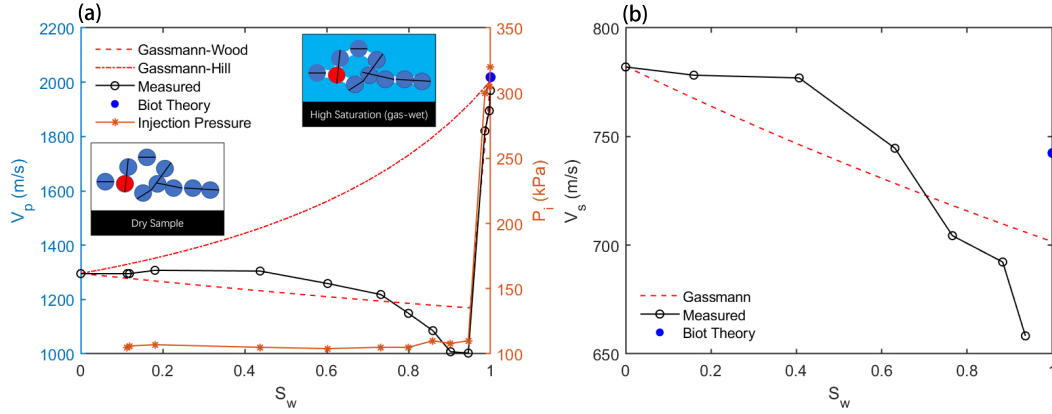


Figure 6. Velocity-saturation relation in gas-wetting glass bead packing vs Gassmann-Wood and Gassmann-Hill predictions for (a) P -Wave and (b) S -Wave. The last three measurements in high water saturation are obtained after increasing 300% injection pressure P_i . The inset cartoons demonstrate the network of force chain (black solid line) in dry and high to near fully saturated samples.

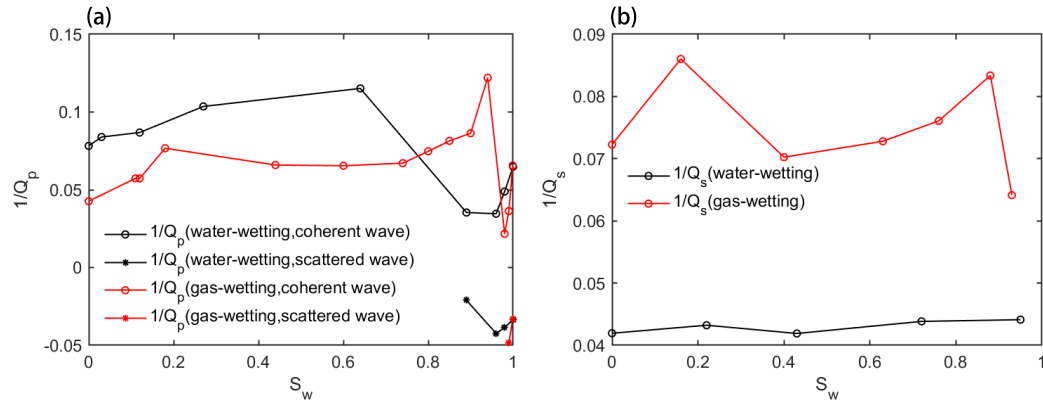


Figure 7. Attenuation-saturation relation of (a) P -wave and (b) S -wave for both water-wetting and gas-wetting samples.

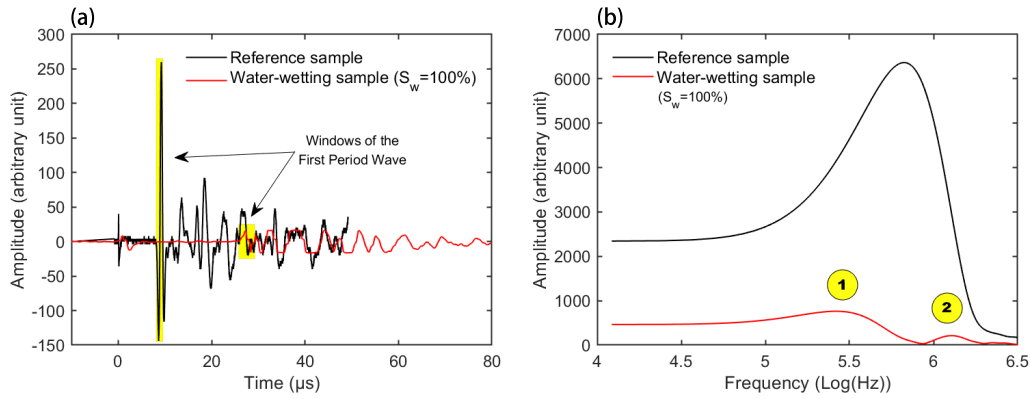


Figure 8. (a) The waveforms through the reference sample (aluminum dummy core) and water-wetting sample with 100% water saturation where the time windows of the first period of waveforms are selected (shading highlight) for calculating the amplitude spectrum in each sample; (b) the corresponding spectra by Fourier transform where two peaks are produced in the spectrum of signals in fully saturated water-wetting sample.

292

4.2 Gas-wetting Case

293

294

295

296

297

298

299

300

301

302

303

Our hypothesis is that only the fluid between the grain contacts has significant impact on the force chain network and therefore on the effective bulk moduli of the matrix frame. For the gas-wetting case, air as wetting-fluid tends to occupy the grain contacts while water is forced into the relatively large interstitial pores from the beginning to the end of the water injection (inset of Figure 6). Since the bulk modulus of the air in the grain contacts of the gas-wetting glass beads is negligibly small we expect no significant change of the structure of the force chain network and the effective moduli of the matrix frame during the water flooding. The measured P -wave VSR coincidentally agrees with the predictions of Gassmann-Wood limit but is far away from Gassmann-Hill prediction. This indicates that the two immiscible fluids tend to be in a homogeneous mixing condition rather than forming patchy fluid pockets (Figure 6).

304

305

306

307

308

309

310

311

The water saturation stops increasing at about 93-94% in the normal water flooding procedure with about 6% residual gas saturation for the gas-wetting sample. Only when we increased the injection pressure by about 300% in an attempt to overcome the capillary pressure, the non-wetting water was pushed into some of the grain contacts. In our interpretation, this should lead to a force chain reinforcement. This is supported by the observation of small amplitude "scattered" waves, which in fact contain both coherent part and incoherent part (Figure 9b). Their P -wave attenuation obtained by the spectral-ratio method is as similar to the scenario of the water-wetting sample.

312

4.3 The Role of Wettability in P -wave Transmission

313

314

315

316

317

There is only one coherent pulse observed in the S -wave transmission experiments regardless the saturation condition and the wettability of the samples. In contrast, in the P -wave transmission experiments, there is a transition from the coherent P -wave pulse in the dry samples to the incoherently "scattered" waves in the samples with high water saturation.

318

319

320

The amplitude spectra of P -waves in the fully water-saturated samples are plotted in Figure 8. We observe that the water-wetting spectra contains a low-frequency part and a high-frequency part. Similar experimental observations are reported by Güven et

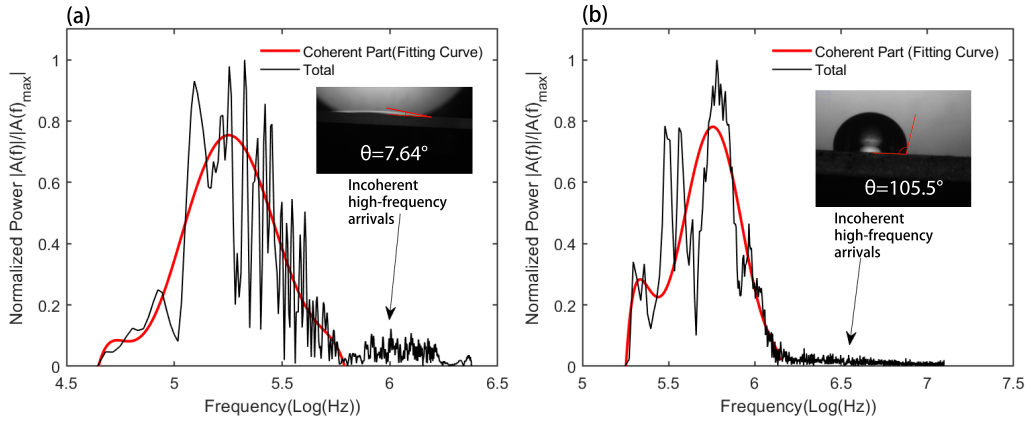


Figure 9. The Amplitude spectra $A(f)$ normalized by the maximum value for the fully saturated (a) water-wetting and (b) gas-wetting glass bead packings. The insets of figures show the contact angle of water droplet on the glass-air interface.

321 al. (2018) and Jia et al. (1999). However, the incoherent arrivals in the spectra of gas-
 322 wetting sample are rare and small. We project that the fluid in the grain contacts plays
 323 a crucial role in the continuity of the force chains, where the liquid promotes the devel-
 324 opment of long force chains as in the water-wetting glass bead packing, but the gas, i.e.,
 325 air restrains the extension of the force chains as in the gas-wetting glass bead packing.
 326 In this way, the wettability is identified to have significant impact on the force chain net-
 327 work by controlling the intergranular fluid distribution, which further determine the wave
 328 velocity, attenuation and scattering.

329 5 Discussion

330 5.1 Path Effect on the Acoustics of Porous Granular Media

331 When the wetting phase fluid is injected into the dry granular porous medium, it
 332 percolates through the pore space and occupies relatively small voids (i.e., grain contacts)
 333 in sequence. In this way, the force chains are extended and re-organized. However, it is
 334 unlikely that the percolation process proceeds such that a homogeneous force chain pat-
 335 tern (FCP) is generated. This should be especially true when the capillary pressure is
 336 small and the impact of gravity on the fluid distribution become considerable. In the fol-
 337 lowing we explore some of the factors that may be responsible for the generation of het-
 338 erogeneous FCPs, which in turn could explain the wavefield signatures observed from
 339 ultrasonic experimentation.

340 We hypothesize that heterogeneous FCP may occur during the injection such that
 341 the notion of an effective medium is no longer valid and instead the heterogeneous FCP
 342 gives rise to preferential wave (ray) paths, i.e., the path effect. To verify this hypothe-
 343 sis and investigate the path effect in porous granular media, we repeat the experiment
 344 as described in Section 2 but introduce two changes. First, we inject decane instead of
 345 water as the wetting phase fluid. The benefit of decane over water is that the decane has
 346 smaller interfacial tension in air ($\sigma = 24.47\text{mN/m}$) compared to water ($\sigma = 72\text{mN/m}$) (Rolo
 347 et al., 2002). The glass bead surface has similar wettability to the decane as to the wa-
 348 ter in the air with a contact angle of less than 10° so that the capillary pressure $P_c =$
 349 $2\sigma \cos \theta / r$ for the decane-air system is only about 1/3 of the water-air system. Hence,
 350 the interplay between capillary forces and gravity (the sample in Figure 1 is oriented hor-

351 horizontally) should be more pronounced, thereby generating a more favorable condition for
 352 FCP generation.

353 Second, we use a shorter sample of length $L = 2.8\text{cm}$ (roughly half of the length
 354 of the original sample; Figure 1). Because the shorter sample is used in the decane in-
 355 jection experiment, a portion of the heterogeneous decane saturation front is likely to
 356 reach the receiver early-on in the fluid injection experiment, say at low to moderate de-
 357 cane saturation. This is indeed observed experimentally (Figure 10a). It is thought that
 358 this heterogeneous saturation front creates different ray paths for ultrasonic waves (Fig-
 359 ure 10b), thereby increasing the level of heterogeneity of the FCP. Specifically, the con-
 360 tinuously decane saturated regions constitutes a distinguished fast ray path along which
 361 the high frequency waves travel. Since the FCP in the saturated regions is thought to
 362 be accompanied with larger characteristic lengths, these fast rays are scattered at clus-
 363 ters. The dry and the low saturation regions correspond to slow ray path along which
 364 mainly the low-frequency part of the broadband waves propagates. This leads to a de-
 365 formation of the wave front and bias towards larger velocity by picking the first break
 366 as illustrated in Figure 10b. Such deformed wave front accounts for the mechanism of
 367 fast path dispersion or velocity shift (Cadoret et al., 1995; Mukerji et al., 1995). This
 368 could explain the recorded P -waveforms at intermediate saturation (i.e., $S_o = 58\%$ and
 369 $S_o = 64\%$) in the decane injection experiment, where two types of wave arrivals with
 370 different frequencies are recorded in the same wave train (Figure 11).

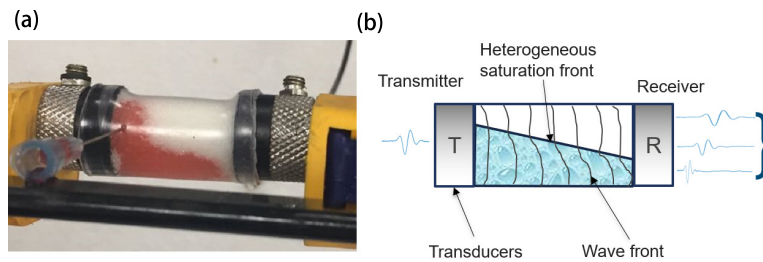


Figure 10. (a) Different ray paths are produced during the injection of liquid into the short sample ($L=2.8\text{cm}$). (b) This schematic shows the path effect on the receiving signals with broadband frequencies where the short wavelength (high-frequency) wave tends to follow the fastest ray path.

371 5.2 Effect of Micro-slip Between Grains

372 It is worth noting that the velocities of both P - and S -wave drop to values lower
 373 than the Gassmann predication at high saturation (from about 75% to 93%) in the gas-
 374 wetting sample but not in the water-wetting sample (Figure 6). This drop might be ex-
 375 plained by micro-slip (sliding) between glass beads as suggested by Makse et al. (2004)
 376 and Langlois and Jia (2014). This leads to an increase of the tangential friction (dissi-
 377 pation) since we see a similar pattern of increasing attenuation in both P - and S -wave
 378 at moderate to high water saturation in the gas-wetting sample (Figure 7). Such micro-
 379 slip also results in a drop in the velocities where the attenuation increases. The occur-
 380 rence of micro-slip due to the grain sliding may be dependent on the wettability and wa-
 381 ter saturation. A further investigation will be required to answer this question.

382 5.3 Comparison with Literature

383 As shown in the experimental results section, we observe a dramatic change in the
 384 waveforms during the change of the fluid saturation in porous granular media. It is in-

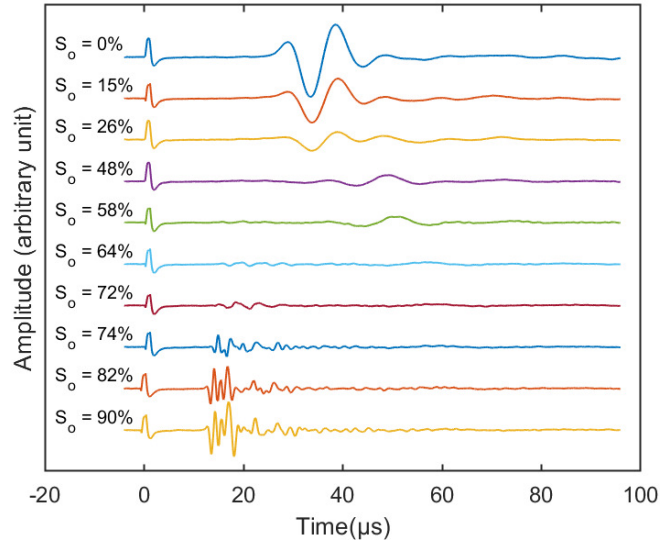


Figure 11. Recorded P -waveforms with incremental decane (oil) injection for shorter glass-bead packings ($L=2.8\text{cm}$). Two types of signals with different frequencies are recorded in the same wave trains at intermediate saturations (i.e. $S_o = 58\%$ and $S_o = 64\%$)

385 interesting to note that a similar phenomenon is documented by C. Sayers and Dahlin (1993)
 386 (their Figure 12). The time-lapse waveform changes from high-frequency (short-period)
 387 arrivals when the sample is in the state of a cement paste (suspension of cement arti-
 388 cles in water) to low-frequency (long-period) waves when sample becomes a cemented
 389 solid (saturated porous media). These waveform changes are caused by the structural
 390 changes during hydration and, compared to our results, the transition of the acoustic wave-
 391 form has a reverse sequence. Since in the cement paste the interconnected chains of ce-
 392 ment particles develop as a function of time, their observations may relate to our inter-
 393 pretation in terms of the reinforced force chains due to the presence of the intergranu-
 394 lar fluid.

395 6 Conclusions

396 The velocity- and attenuation-saturation relations and P -wave scattering patterns
 397 in the water-wetting and gas-wetting granular porous media examined here show distinct
 398 characteristics. This indicates that the wettability has a significant impact on the wave
 399 propagation in the granular porous medium. We explain these characteristics in terms
 400 of wettability-dependent force chain network alterations. In particular, the effective elas-
 401 tic moduli and the characteristic length of force chain network are altered during the wa-
 402 ter injection. The dry granular porous medium, as an extreme example, where all pores
 403 are saturated by air, has a short-range characteristic length. It behaves as an effective
 404 medium in which a stable pulse waveform is observed. For partial saturation, only if the
 405 water wets the grains, the liquid can intrude the small grain contacts. Therefore, the grain
 406 contact-filling fluid as wetting phase (i.e., water) results in the development of the longer-
 407 range force chains and higher effective moduli. This appears to be a plausible explan-
 408 ation of the wave velocities, that exceed the prediction of the Gassmann theory, and the
 409 appearance of shorter pulses comprising a more complex wave train.

Appendix A Gassmann-Wood and Gassmann-Hill limits for partially saturated sample

The velocity of the P - and S -wave for the sample saturated by a single fluid can be calculated as,

$$V_p = \sqrt{\frac{K + \frac{4}{3}\mu}{\rho}}; \quad (\text{A1})$$

$$V_s = \sqrt{\frac{\mu}{\rho}}; \quad (\text{A2})$$

K : bulk modulus of the fully saturated sample
 μ : shear modulus of the fully saturated sample
 ρ : density of the fully saturated sample

The K and μ can be derived by the Gassmann equations,

$$\frac{K}{K_s - K} = \frac{K_d}{K_s - K_d} + \frac{K_f}{\phi(K_s - K_f)} \quad (\text{A3})$$

$$\mu = \mu_d \quad (\text{A4})$$

K_s : bulk modulus of solid
 K_d : bulk modulus of the drained matrix (dry) frame
 K_f : bulk modulus of fluid
 ϕ : porosity
 μ_d : shear modulus of the drained matrix (dry) frame

Gassmann-Wood lower bound limit applying the Wood law to determine the effective fluid bulk modulus K_f which can be further applied to determine the bulk modulus of partially saturated sample ($K_{GW} = K$) by Eq. (A3) and the velocity by Eq. (A1),

$$\frac{1}{K_f} = \frac{S_w}{K_w} + \frac{1 - S_w}{K_g} \quad (\text{A5})$$

S_w is the water saturation; K_w and K_g are the bulk moduli of the water and gas, respectively.

Gassmann-Hill upper bound limit uses the Hill average bulk modulus of the partially saturated sample K which can be further used in to calculate the velocity by Eq. (A1),

$$\frac{1}{K + \frac{4}{3}\mu} = \frac{S_w}{K_1 + \frac{4}{3}\mu} + \frac{1 - S_w}{K_2 + \frac{4}{3}\mu} \quad (\text{A6})$$

K_1 , K_2 are the bulk moduli of the sample fully saturated by water and gas, respectively.

In either Gassmann-Wood or -Hill limit calculation, the density of the composite partially saturation sample is,

$$\rho = \rho_s(1 - \phi) + (\rho_w S_w + \rho_g - \rho_g S_w)\phi \quad (\text{A7})$$

ρ_w , ρ_g are the density of the water and gas, respectively.

The Mavko-Jizba relations use the bulk modulus K_{uf} and shear modulus μ_{uf} of the unrelaxed frame to replace the K_d and μ_d in the Gassmann equations (Eq. (A3) and (A4)) to calculate the moduli of the fully saturated sample ($K_{MJ} = K$; $\mu_{MJ} = \mu = \mu_{uf}$) and the corresponding velocities by Eq. (A1) and (A2).

$$\frac{1}{K_{uf}} \approx \frac{1}{K_h} + \left(\frac{1}{K_f} - \frac{1}{K_s}\right)\phi_s \quad (\text{A8})$$

$$\left(\frac{1}{\mu_{uf}} - \frac{1}{\mu_d}\right) = \frac{4}{15} \left(\frac{1}{K_{uf}} - \frac{1}{K_d}\right) \quad (\text{A9})$$

450
451 ϕ_s : soft porosity or the porosity that closes at high pressure; $\phi_s = \phi/50$ is used
452 in the simulation. K_h : effective bulk modulus of dry sample at high pressure when the
453 soft porosity is compressed to close; $K_h = \pi K_d$ is used in the simulation. As the $K_d \propto$
454 $P^{\frac{1}{3}}$ according to the Hertz-Mindlin theory, the K_h is approximated to the bulk modu-
455 lus of the dry granular glassbead packing under confining pressure $P \approx 0.15 \times \pi^3 \approx$
456 5 MPa , which is a reasonable confining pressure to suppress the soft porosity.

457 Appendix B Attenuation Estimation by Spectral-Ratio Method

458 The P - and S -wave attenuation (inverse quality factor) in glass bead packings are
459 calculated by the spectral-ratio method (Toksöz et al., 1979). The ratio of amplitudes
460 for the reference aluminum core and the sample is given as

$$\ln\left(\frac{A_1}{A_2}\right) = (\gamma_2 - \gamma_1)Lf + \ln\left(\frac{G_1}{G_2}\right), \quad (\text{B1})$$

462 where A is the Fourier amplitude, γ is the attenuation coefficient, f is the frequency, and
463 G denotes the geometrical spreading factor. Subscripts 1 and 2 indicate the sample and
464 reference, respectively. $\ln(G_1/G_2)$ is a constant due to the sample and reference have the
465 same shape and size. The sample length L and can be obtained from the direct measure-
466 ment. The quality factor Q related to the attenuation coefficient can be expressed as

$$Q = \frac{\pi}{\gamma v}, \quad (\text{B2})$$

468 where v is the phase velocity. Since Q of the reference sample is very high, γ_2 can be con-
469 sidered as 0, which only introduces an error of less than 1%. Thus, Eq. (B1) can be writ-
470 ten as

$$\ln\left(\frac{A_1}{A_2}\right) = \frac{-\pi L}{Q_1 v} + \ln\left(\frac{G_1}{G_2}\right). \quad (\text{B3})$$

472 The attenuation of sample (Q_1^{-1}) can be estimated from the slope of the linear fitting
473 of $\ln\left(\frac{A_1}{A_2}\right)$ versus the frequency.

474 Acknowledgments

475 This study was supported by an Australian Government Research Training Program (RTP)
476 Scholarship. J. Li thanks Dr. Faaiz Al-Shajalee for the microscopy images and Dr. Nilesh
477 Kumar for the training of IFT and contact angle measurements. T. Müller acknowledges
478 the support of the Jiangsu 100 Plan of Foreign Experts.

479 **Data availability:** The waveform data are available at: <https://doi.org/10.5281/zenodo.4665478>.

480 References

- 481 Alemu, B. L., Aker, E., Soldal, M., Johnsen, Ø., & Aagaard, P. (2013). Effect
482 of sub-core scale heterogeneities on acoustic and electrical properties of a
483 reservoir rock: a CO₂ flooding experiment of brine saturated sandstone in a
484 computed tomography scanner. *Geophysical Prospecting*, *61*(1), 235–250.
- 485 Anderson, W. G. (1987). Wettability literature survey part 5: The effects of wetta-
486 bility on relative permeability. *Journal of Petroleum Technology*, *39*(11), 1453–
487 1468.
- 488 Anderson, W. G., et al. (1986). Wettability literature survey-part 1: rock/oil/brine
489 interactions and the effects of core handling on wettability. *Journal of*
490 *petroleum technology*, *38*(10), 1–125.

- 491 Anderson, W. G., et al. (1987a). Wettability literature survey-part 4: Effects of wet-
492 tability on capillary pressure. *Journal of petroleum technology*, 39(10), 1–283.
- 493 Anderson, W. G., et al. (1987b). Wettability literature survey-part 6: the effects of
494 wettability on waterflooding. *Journal of petroleum technology*, 39(12), 1–605.
- 495 Anthony, J. L., & Marone, C. (2005). Influence of particle characteristics on granu-
496 lar friction. *Journal of Geophysical Research: Solid Earth*, 110(B8).
- 497 Ba, J., Carcione, J., & Nie, J. (2011). Biot-rayleigh theory of wave propagation
498 in double-porosity media. *Journal of Geophysical Research: Solid Earth*,
499 116(B6).
- 500 Berryman, J. G., & Thigpen, L. (1985). Effective constants for wave propagation
501 through partially saturated porous media. *Applied Physics Letters*, 46(8), 722–
502 724.
- 503 Brunet, T., Jia, X., & Mills, P. (2008). Mechanisms for acoustic absorption in dry
504 and weakly wet granular media. *Physical review letters*, 101(13), 138001.
- 505 Bultreys, T., Van Hoorebeke, L., & Cnudde, V. (2016). Simulating secondary water-
506 flooding in heterogeneous rocks with variable wettability using an image-based,
507 multiscale pore network model. *Water Resources Research*, 52(9), 6833–6850.
- 508 Cadoret, T., Marion, D., & Zinszner, B. (1995). Influence of frequency and fluid dis-
509 tribution on elastic wave velocities in partially saturated limestones. *Journal of*
510 *Geophysical Research: Solid Earth*, 100(B6), 9789–9803.
- 511 Daniels, K. E., & Hayman, N. W. (2008). Force chains in seismogenic faults visual-
512 ized with photoelastic granular shear experiments. *Journal of Geophysical Re-*
513 *search: Solid Earth*, 113(B11).
- 514 Davis, R. H., Serayssol, J.-M., & Hinch, E. (1986). The elasto-hydrodynamic collision
515 of two spheres. *Journal of Fluid Mechanics*, 163, 479–497.
- 516 Dutta, N., & Odé, H. (1979). Attenuation and dispersion of compressional waves
517 in fluid-filled porous rocks with partial gas saturation (white model)—part ii:
518 Results. *Geophysics*, 44(11), 1789–1805.
- 519 Dutta, T., Mavko, G., & Mukerji, T. (2010). Improved granular medium model
520 for unconsolidated sands using coordination number, porosity, and pressure
521 relations. *Geophysics*, 75(2), E91–E99.
- 522 Dvorkin, J., Mavko, G., & Nur, A. (1991). The effect of cementation on the elastic
523 properties of granular material. *Mechanics of Materials*, 12(3-4), 207–217.
- 524 Dvorkin, J., Nur, A., & Yin, H. (1994). Effective properties of cemented granular
525 materials. *Mechanics of materials*, 18(4), 351–366.
- 526 Garrouch, A. A., & Alikhan, A. A. (1997, 06). *An Improved Method For Quantifying*
527 *In-Situ Intermediate Wettability Using Well Logs* (Vol. All Days). (SPWLA-
528 1997-Z)
- 529 Garrouch, A. A., & Sharma, M. M. (1995). Dielectric properties of partially satu-
530 rated rocks. *Energy & Fuels*, 9(3), 413–419. doi: 10.1021/ef00051a004
- 531 Griffiths, S., Rescaglio, A., & Melo, F. (2010). Ultrasound propagation in wet and
532 airless non-consolidated granular materials. *Ultrasonics*, 50(2), 139–144.
- 533 Güven, I., Luding, S., & Steeb, H. (2018). Incoherent waves in fluid-saturated sin-
534 tered granular systems: Scattering phenomena. *Journal of vibration and acous-*
535 *tics*, 140(1).
- 536 Howell, D., Behringer, R. P., & Veje, C. (1999). Stress fluctuations in a 2d granular
537 couette experiment: a continuous transition. *Physical Review Letters*, 82(26),
538 5241.
- 539 Hu, R., Wan, J., Kim, Y., & Tokunaga, T. K. (2017). Wettability impact on super-
540 critical co2 capillary trapping: Pore-scale visualization and quantification. *Wa-*
541 *ter Resources Research*, 53(8), 6377–6394.
- 542 Jia, X., Caroli, C., & Velicky, B. (1999). Ultrasound propagation in externally
543 stressed granular media. *Physical Review Letters*, 82(9), 1863.
- 544 Job, S., Santibanez, F., Tapia, F., & Melo, F. (2008). Nonlinear waves in dry and
545 wet hertzian granular chains. *Ultrasonics*, 48(6-7), 506–514.

- 546 Johnson, D. L. (2001). Theory of frequency dependent acoustics in patchy-saturated
547 porous media. *The Journal of the Acoustical Society of America*, *110*(2), 682–
548 694.
- 549 Johnson, P. A., & Jia, X. (2005). Nonlinear dynamics, granular media and dynamic
550 earthquake triggering. *Nature*, *437*(7060), 871–874.
- 551 Khishvand, M., Alizadeh, A., Kohshour, I. O., Piri, M., & Prasad, R. (2017). In situ
552 characterization of wettability alteration and displacement mechanisms govern-
553 ing recovery enhancement due to low-salinity waterflooding. *Water Resources*
554 *Research*, *53*(5), 4427–4443.
- 555 Ladd, C. R., & Reber, J. E. (2020). The effect of a liquid phase on force distribu-
556 tion during deformation in a granular system. *Journal of Geophysical Research:*
557 *Solid Earth*, *125*(8), e2020JB019771.
- 558 Langlois, V., & Jia, X. (2014). Acoustic probing of elastic behavior and damage in
559 weakly cemented granular media. *Physical Review E*, *89*(2), 023206.
- 560 Lebedev, M., Toms-Stewart, J., Clennell, B., Pervukhina, M., Shulakova, V., Pa-
561 terson, L., . . . Wenzlau, F. (2009). Direct laboratory observation of patchy
562 saturation and its effects on ultrasonic velocities. *The Leading Edge*, *28*(1),
563 24–27.
- 564 Liu, C.-h., & Nagel, S. R. (1992). Sound in sand. *Physical review letters*, *68*(15),
565 2301.
- 566 Liu, J., Müller, T. M., Qi, Q., Lebedev, M., & Sun, W. (2016). Velocity-saturation
567 relation in partially saturated rocks: Modelling the effect of injection rate
568 changes. *Geophysical Prospecting*, *64*(4-Advances in Rock Physics), 1054–
569 1066.
- 570 Lo, W.-C., & Sposito, G. (2013). Acoustic waves in unsaturated soils. *Water Re-*
571 *sources Research*, *49*(9), 5674–5684.
- 572 Lo, W.-C., Sposito, G., & Majer, E. (2005). Wave propagation through elastic
573 porous media containing two immiscible fluids. *Water Resources Research*,
574 *41*(2).
- 575 Lo, W.-C., Yang, C.-C., Hsu, S.-Y., Chen, C.-H., Yeh, C.-L., & Hilpert, M. (2017).
576 The dynamic response of the water retention curve in unsaturated soils during
577 drainage to acoustic excitations. *Water Resources Research*, *53*(1), 712–725.
- 578 Lopes, S., Lebedev, M., Müller, T. M., Clennell, M. B., & Gurevich, B. (2014).
579 Forced imbibition into a limestone: Measuring p-wave velocity and water
580 saturation dependence on injection rate. *Geophysical Prospecting*, *62*(5),
581 1126–1142.
- 582 Makse, H. A., Gland, N., Johnson, D. L., & Schwartz, L. (2004). Granular packings:
583 Nonlinear elasticity, sound propagation, and collective relaxation dynamics.
584 *Physical Review E*, *70*(6), 061302.
- 585 Mavko, G., & Jizba, D. (1991). Estimating grain-scale fluid effects on velocity dis-
586 persion in rocks. *Geophysics*, *56*(12), 1940–1949.
- 587 Mavko, G., & Mukerji, T. (1998). Bounds on low-frequency seismic velocities in par-
588 tially saturated rocks. *Geophysics*, *63*(3), 918–924.
- 589 Melosh, H. (1996). Dynamical weakening of faults by acoustic fluidization. *Nature*,
590 *379*(6566), 601–606.
- 591 Moebius, F., Canone, D., & Or, D. (2012). Characteristics of acoustic emissions in-
592 duced by fluid front displacement in porous media. *Water Resources Research*,
593 *48*(11).
- 594 Mukerji, T., Mavko, G., Mujica, D., & Lucet, N. (1995). Scale-dependent seismic ve-
595 locity in heterogeneous media. *Geophysics*, *60*(4), 1222–1233.
- 596 Müller, T. M., & Gurevich, B. (2004). One-dimensional random patchy saturation
597 model for velocity and attenuation in porous rocks random patchy saturation
598 model. *Geophysics*, *69*(5), 1166–1172.
- 599 Murphy III, W. F. (1984). Acoustic measures of partial gas saturation in tight sand-
600 stones. *Journal of Geophysical Research: Solid Earth*, *89*(B13), 11549–11559.

- 601 Nagy, P. B., & Blaho, G. (1994). Experimental measurements of surface stiffness on
 602 water-saturated porous solids. *The Journal of the Acoustical Society of Amer-*
 603 *ica*, *95*(2), 828–835.
- 604 Owens, E. T., & Daniels, K. E. (2011). Sound propagation and force chains in gran-
 605 ular materials. *EPL (Europhysics Letters)*, *94*(5), 54005.
- 606 Parra, J. O., Hackert, C. L., & Bennett, M. W. (2006). Permeability and porosity
 607 images based on p-wave surface seismic data: Application to a south florida
 608 aquifer. *Water Resources Research*, *42*(2).
- 609 Qi, Q., Müller, T. M., Gurevich, B., Lopes, S., Lebedev, M., & Caspari, E. (2014).
 610 Quantifying the effect of capillarity on attenuation and dispersion in patchy-
 611 saturated rocks. *Geophysics*, *79*(5), WB35–WB50.
- 612 Rolo, L. I., Caco, A. I., Queimada, A. J., Marrucho, I. M., & Coutinho, J. A. (2002).
 613 Surface tension of heptane, decane, hexadecane, eicosane, and some of their
 614 binary mixtures. *Journal of Chemical & Engineering Data*, *47*(6), 1442–1445.
- 615 Santos, J. E., Douglas Jr, J., Corberó, J., & Lovera, O. M. (1990). A model for wave
 616 propagation in a porous medium saturated by a two-phase fluid. *The Journal*
 617 *of the Acoustical Society of America*, *87*(4), 1439–1448.
- 618 Sayers, C., & Dahlin, A. (1993). Propagation of ultrasound through hydrating ce-
 619 ment pastes at early times. *Advanced Cement Based Materials*, *1*(1), 12–21.
- 620 Sayers, C. M. (2021). Mechanical properties of grain contacts in unconsolidated
 621 sands. *Geophysics*, *86*(2), MR95–MR103.
- 622 Scott, D. R. (1996). Seismicity and stress rotation in a granular model of the brittle
 623 crust. *Nature*, *381*(6583), 592–595.
- 624 Sun, W., Xiong, F., Ba, J., & Carcione, J. M. (2018). Effects of ellipsoidal het-
 625 erogeneities on wave propagation in partially saturated double-porosity rocks.
 626 *Geophysics*, *83*(3), WC71–WC81.
- 627 Toksöz, M., Johnston, D. H., & Timur, A. (1979). Attenuation of seismic waves in
 628 dry and saturated rocks: I. laboratory measurements. *Geophysics*, *44*(4), 681–
 629 690.
- 630 Toms, J., Müller, T., Ciz, R., & Gurevich, B. (2006). Comparative review of theo-
 631 retical models for elastic wave attenuation and dispersion in partially saturated
 632 rocks. *Soil Dynamics and Earthquake Engineering*, *26*(6-7), 548–565.
- 633 Tserkovnyak, Y., & Johnson, D. L. (2003). Capillary forces in the acoustics of
 634 patchy-saturated porous media. *The Journal of the Acoustical Society of*
 635 *America*, *114*(5), 2596–2606.
- 636 White, J. (1975). Computed seismic speeds and attenuation in rocks with partial gas
 637 saturation. *Geophysics*, *40*(2), 224–232.
- 638 Xu, P., & Yu, B. (2008). Developing a new form of permeability and kozeny–carman
 639 constant for homogeneous porous media by means of fractal geometry. *Ad-*
 640 *vances in water resources*, *31*(1), 74–81.